Tight-Binding Total Energy Methods for Magnetic Materials and Multi-element Systems

(June 17, 2005)

The classic paper of Slater and Koster [1] described a method for modifying a linear combination of atomic orbitals (LCAO) for use in an interpolation scheme to determine energy bands over the entire Brillouin zone while only fitting to the results of first-principles calculations at high symmetry points in the zone. This Tight-Binding (TB) method was shown to be extremely useful for the study of the band structure of solids with little computational cost. Harrison[2, 3] developed a "universal" set of parameters which are used both to obtain a basic understanding of band structures and for making approximate calculations. Papaconstantopoulos[4] computed the Slater-Koster parameters for most elements by fitting to results obtained from the first-principles Augmented Plane Wave (APW) method. Numerous other applications of this method have appeared in the literature.[5, 6]

As computational methods developed, it was realized[7, 8, 9, 10, 11] that tight-binding methods, properly applied, could be used as scheme for determining structural energies as well as electronic structure. Since these methods use a minimal basis set for each atom, they are much faster than first-principles methods for similar size systems, and therefore useful for quickly studying systems containing several hundred atoms, *e.g.* in molecular dynamics simulations.[12]

One example of the method is the two-center, non-orthogonal NRL-TB method,[9, 10] which uses environment-dependent on-site parameters and bond-length dependent hopping parameters to go beyond interpolating between fitted structures to the determination of elastic constants, phonon spectra, and defect structures. A similar approach is used by the Ames group[11, 13, 14] who approximate the three-center integrals by modifying the two-center hopping integrals according to the local environment. Cohen, Stixrude, and Wasserman[15] have modified the description of the on-site parameters (4-6) to include crystal-field like corrections, extending the work of Mercer and Chou[16] to include d orbitals. We have previously summarized much of this work.[5, 6] In this article we focus on extensions of the TB method beyond the original elemental systems. Specifically, we show how the method can be extended to spin-polarized systems, including non-collinear spins, using the Atomic Moment Approximation (AMA).[17] We also describe the development of parameters

for binary and ternary compounds.

As we will see, although the determination of the TB parameters is tedious, the resulting method is computationally efficient, capable of performing static and dynamic calculations beyond the limits of first-principles methods. The method has been applied to all of the magnetic elements, and many non-magnetic compounds. The accuracy of electronic, elastic, and phonon properties is comparable to that of the original, non-magnetic single element calculations.

In the discussion of our work below, our tight-binding calculations are fitted to first principles results obtained from the Linearized Augmented Plane Wave (LAPW) method,[18] including full potential and total energy capabilities.[19, 20] Calculations used the Kohn-Sham independent electron formulation of Density Functional Theory[21, 22] with various Local Density Approximations (LDA)[23] or the Perdew-Wang 1991 Generalized Gradient Approximation (GGA).[24] Other tight-binding methods use similar first-principles techniques, as described in the references.

This work is divided into two major parts. Section I describes work on spin polarized systems, including non-collinear spins, while Section II shows how tight-binding methods can be adapted to compounds. Finally, in Section III we briefly discuss the future of tight-binding total energy methods.

I. MAGNETIC SYSTEMS

Since spin-polarized density functional calculations produce eigenvalues for both the majority and minority spin channels, it is rather easy to set up a Slater-Koster tight-binding parametrization for each channel. These parameter sets are bound together by the requirement that they reproduce the first-principles eigenvalues for each spin as well as the total energy. Accordingly, we modify the original non-polarized tight-binding procedure[9, 10] as follows:

The total energy of the tight-binding system is given by the sum over occupied states of the shifted spin-polarized eigenvalues:

$$E = \sum_i f(\varepsilon'_{i\uparrow} - \mu')\varepsilon'_{i\uparrow} + \sum_i f(\varepsilon'_{i\downarrow} - \mu')\varepsilon'_{i\downarrow} \ , \tag{1}$$

where $f(\varepsilon)$ is a smoothing function, usually the Fermi function,[25] and μ' is the shifted

Fermi level, which gives the correct number of occupied bands, and the arrows indicate the collinear spin-polarization of the electronic states. The eigenvalues ε' are uniformly shifted from the eigenvalues ε found from the density functional calculations:

$$\begin{aligned} \varepsilon'_{i\uparrow} &= \varepsilon_{i\uparrow} + \varepsilon_s \ , \text{ and} \\ \varepsilon'_{i\downarrow} &= \varepsilon_{i\downarrow} + \varepsilon_s \ . \end{aligned} \tag{2}$$

The shift, ε_s, is defined so that the total energy E in (1) is equal to the total energy from the DFT calculation:

$$\varepsilon_s = \{E - \sum_i [f(\varepsilon_{i\uparrow} - \mu)\varepsilon_{i\uparrow} + \sum_i f(\varepsilon_{i\downarrow} - \mu)\varepsilon_{i\downarrow}\}/N_e \ , \tag{3}$$

where N_e is the number of electrons in the system and $\mu = \mu' + \varepsilon_s$ is the Fermi level for the original DFT calculation.

In our approach to spin-polarized tight-binding[26] we assign all of the difference between the majority and minority bands to the on-site terms. Thus with each atom i we associate both a majority and a minority "density" of nearby atoms:

$$\rho_{i(\uparrow,\downarrow)} = \sum_j \exp(-\lambda^2_{\uparrow,\downarrow} R_{i,j}) \mathcal{F}(R_{ij}), \tag{4}$$

where

$$\mathcal{F}(R) = \theta(R_c - R)/\{1 + \exp[(R - R_c)/L + 5]\} \ , \tag{5}$$

is a screening function designed to smoothly take the densities (4) to zero at distances greater than R_c. Typically we take R_c between 10 and 16 a.u., and L between 0.25 and 0.5 a.u.

Once we have the density in the neighborhood of each atom, we assign the spin-dependent on-site parameters for states with angular momentum $\ell = s, p$, and d by

$$h_{i\ell(\uparrow,\downarrow)} = \alpha_{\ell(\uparrow,\downarrow)} + \beta_{\ell(\uparrow,\downarrow)} \rho^{2/3}_{i(\uparrow,\downarrow)} + \gamma_{\ell(\uparrow,\downarrow)} \rho^{4/3}_{i(\uparrow,\downarrow)} + \delta_{\ell(\uparrow,\downarrow)} \rho^2_{i(\uparrow,\downarrow)} \ . \tag{6}$$

We will frequently find it useful to determine the energy of a paramagnetic system using these tight-binding parameters. In the paramagnetic system the on-site parameters are the average of the majority and minority spin parameters in (6).

The hopping and on-site terms have the same form here as in our unpolarized tight-binding calculations, and are taken to be independent of the spin associated with each

tight-binding orbital. Thus the Slater-Koster hopping parameters between atoms separated by a distance R are given by

$$H_{\ell\ell'\mu} = [A_{\ell\ell'\mu} + B_{\ell\ell'\mu}R + C_{\ell\ell'\mu}R^2] \exp(-D^2_{\ell\ell'\mu}R)\mathcal{F}(R) \ , \tag{7}$$

where $\ell\ell'\mu = (ss\sigma, sp\sigma, pp\sigma, pp\pi, sd\sigma, pd\sigma, pd\pi, dd\sigma, dd\pi, dd\delta)$ are the Slater-Koster parameters. We usually assume the tight-binding basis to be non-orthogonal, requiring us to define a set of overlap parameters $S_{\ell\ell'\mu}$ to compliment (7). In the spin-polarized calculations we have done so far we have given S the same functional form as H, only noting here that this is not required for a successful theory.[9, 10]

For an sp^3d^5 basis, the procedure above gives 106 independent parameters. For Iron[26] we fit these parameters to reproduce a database of eigenvalues and total energies for paramagnetic bcc Fe, ferromagnetic bcc Fe, and ferromagnetic fcc Fe, using the GGA[24] to obtain the correct ferromagnetic body-centered cubic ground state. The structural energies as a function of volume are shown in Fig. 1, where we compare our results to first-principles calculations. We note that the output paramagnetic fcc total energy closely tracks the paramagnetic fcc energy from LAPW calculations. It should be noted that the tight-binding parametrization cannot reproduce the low-spin/high-spin discontinuity found in ferromagnetic fcc Iron.[27] This is not usually a problem in Fe, especially when we consider that the paramagnetic fcc TB total energy is very close to the low-spin fcc LAPW total energy.

The tight-binding method also lets us examine the total polarization in a system, as the difference in occupation number between the majority and minority spin sites,

$$m = \sum_i [f(\epsilon_{i\uparrow} - \mu) - f(\epsilon_{i\downarrow} - \mu)] \ . \tag{8}$$

Fig. 2 shows the magnetic moment for fcc and bcc Iron as a function of volume. Note that the first-principles high/low spin transition in fcc Iron occurs at approximately the same volume at which the paramagnetic TB total energy becomes lower than the ferromagnetic TB energy for the FCC lattice.

We have extended our tight-binding calculations for magnetic systems to Cobalt and Nickel (as well as Chromium, which will be discussed below). Both elements are substantially easier to fit than Iron, since there is no high/low spin transition in any state. Our fitting database included first-principles LAPW total energy calculations for the fcc, bcc, and simple cubic structures, using the Hedin-Lundqvist LDA.[23] The resulting TB parameters

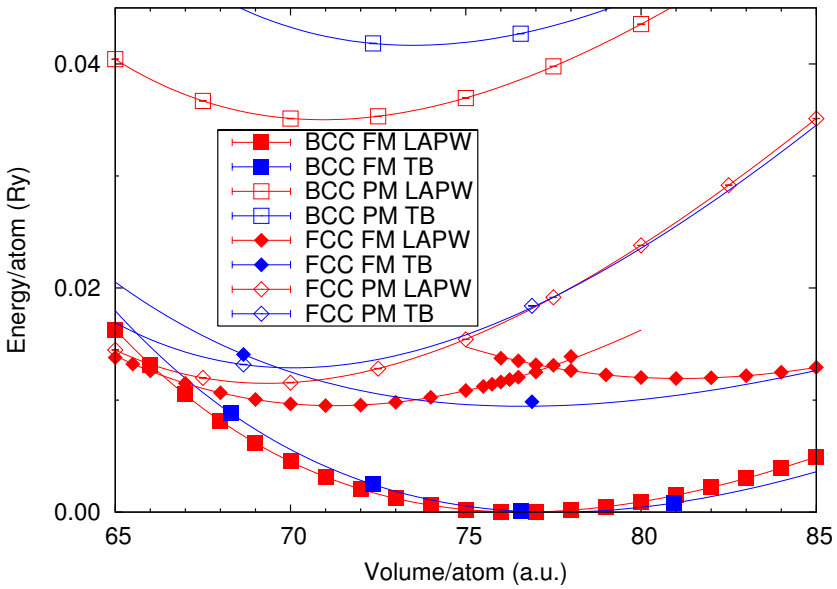

FIG. 1: Comparison for first-principles and tight-binding calculations for Fe, using a spin-polarized tight-binding parametrization.[26] Squares represent bcc phases, diamonds fcc phases. Solid symbols denote ferromagnetic phases, open symbols unpolarized phases. Red lines are LAPW calculations, blue lines tight-binding. The low-spin/high-spin discontinuity in the LAPW ferromagnetic phase is not reproduced by the tight-binding parametrization.

correctly predict the ferromagnetic hcp lattice as the ground state of Co, even though we did not include this state in the fit. Table I shows our calculated elastic constants[28, 29] for the three ferromagnetic elements as well as Cr. We list the TB results at both the equilibrium and experimental volumes.[30] At the experimental volume we find that the elastic constants are in good agreement with experiment, and are at the same level of accuracy as first-principles DFT calculations.

Using our tight-binding parameters we have determined phonon frequencies at high-symmetry locations in the Brillouin zone, using the frozen-phonon method. Table II shows phonon frequencies for Iron and Nickel, compared to experiment.[31, 32] The symmetry notation used here follows that of Miller and Love.[33] We see that the agreement here is comparable to similar calculations for non-magnetic transition metals.[9]

Barreteau *et al.*[34] have developed a method for the study of magnetism in transition metals by starting with an approach similar to ours for the non-magnetic part of the interaction,[35] and modeling the magnetic interactions by a multiband Hubbard model

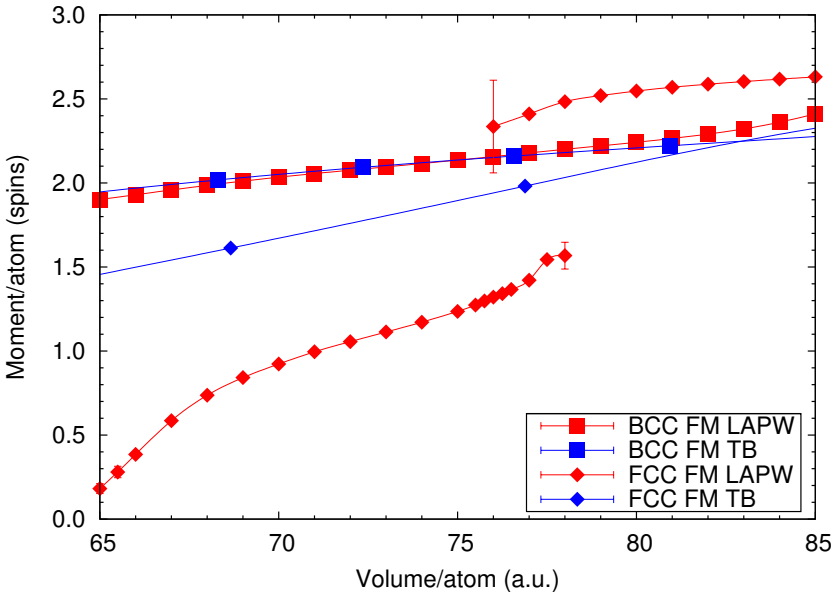

FIG. 2: Comparison for first-principles and tight-binding calculations for the magnetic moment of Fe, using the spin-polarized tight-binding parametrization of Ref. [26]. The notation is the same as in Fig. 1.

treated in the Hartree-Fock approximation. The method has been applied to Rh and Pd clusters and slabs.[36] Recently Barreteau *et al.*[37] analyzed the main effects due to the renormalization of the hopping integrals by the intersite Coulomb interactions. They find that these effects are strongly dependent on the relative values of the intersite electron-electron interaction and on the shape of the electronic density of states. The predicted electronic structure for bcc Iron, hcp Cobalt, and fcc Nickel are in excellent agreement with first-principles calculations.

Xie and Blackman[38] begin with a similar, though orthogonal, form for the non-magnetic part of the tight-binding calculation, and add parametrized terms for charge self-consistency and spin polarization. They use their method to study the magnetics of Iron clusters embedded in Cobalt.

Finally, we note that one could apply the semiempirical approach of Krasko,[39] using a Stoner model to add a magnetization energy to, in our case, a non-magnetic tight-binding parametrization. This approach has the advantage that a single set of parameters serves for both the magnetic and non-magnetic cases, but it has not been applied to materials other than Iron.

TABLE I: Elastic constants for the magnetic elements computed from the spin-polarized tight-binding parameters and compared to experiment.[30] Calculations for Fe, Co, and Ni were done with ferromagnetic spin orientations. The first "TB" column is the tight-binding equilibrium volume, while the second is at the experimental equilibrium. For Co we use the tight-binding minimum energy value for c/a at the experimental volume. As explained in the text, we model the spin-density wave in Chromium by a CsCl type unit cell, where one of the Cr atoms has spin "up" and the other spin "down". All elastic constants are in GPa.

	Cr			Fe			Co			Ni		
	TB	TB	Exp.	TB	TB	Exp.	TB	TB	Exp.	TB	TB	Exp.
a (a.u.)	5.280	5.451	5.451	5.373	5.416	5.416	4.797	4.786	4.743	6.483	6.652	6.652
c (a.u.)							7.591	7.557	7.693			
B	278	164	162	180	158	173	223	247	186	264	175	185
C_{11}	599	407	350	250	223	237	348	359	287	358	251	249
C_{12}	117	42	68	145	125	141	180	189	158	217	137	153
C_{13}							160	168	116			
C_{33}							322	336	322			
C_{44}	142	105	101	142	132	116	78	80	66	75	69	96

We have calculated vacancy formation energies by a supercell method.[10, 25] One atom in the supercell is removed and neighboring atoms are allowed to relax around this vacancy while preserving the symmetry of the lattice. The great advantage of the NRL-TB method over first-principles approaches is that we can do the calculation in a very large supercell, in a computationally efficient manner, including relaxation with the TBMD code.[12] We found that a supercell containing 216 atoms was sufficient to eliminate vacancy-vacancy interactions in ferromagnetic iron and nickel. For iron, we found an unrelaxed vacancy formation energy of 2.62 eV, and a relaxed formation energy of 2.33 eV. For nickel we found 1.87 and 1.60 eV for the unrelaxed and relaxed formation energies. The relaxed vacancy formation energies are in very good agreement with the experimental values of 2.0 eV for iron and 1.6 eV for nickel.

TABLE II: Phonon frequencies at selected high symmetry points for ferromagnetic fcc Iron and bcc Nickel, computed from NRL tight-binding parameters and compared to experiment. Symmetry labels follow the notation of Miller and Love.[33] The column labeled "P" indicates the polarization of the mode, either Longitudinal (L) or Transverse (T), if it is defined. The column "D" indicates the degeneracy of the mode. All frequencies are in inverse centimeters.

Fe					Ni				
Sym.	P	D	TB	Exp.[31]	Sym.	P	D	TB	Exp.[32]
H		3	289	286	X_3	L	1	273	285
P		3	262	240	X_5	T	2	180	209
N_3	L	1	308	357	L_2	L	1	265	296
N_2	T	1	221	215	L_3	T	2	130	141
N_4	T	1	148	149	W_2		1	170	207
					W_5		2	198	250

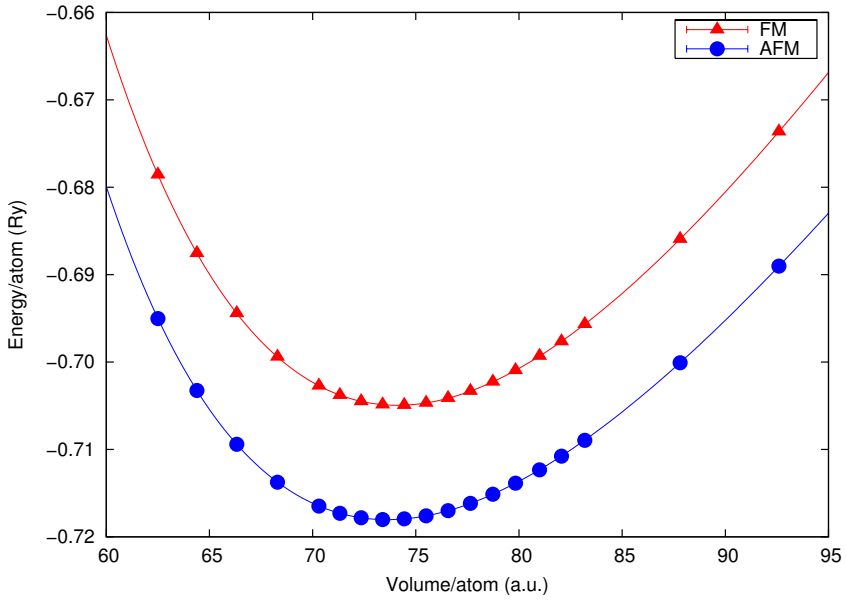

FIG. 3: Tight-binding total energy calculations for bcc Chromium, using spin-polarized parameters. The ferromagnetic (FM) calculations were done in the bcc unit cell. The anti-ferromagnetic (AFM) calculations were performed using two atoms in a simple cubic unit cell, with one spin pointing "up," and the other "down."[40]

A. Non-Collinear Magnetism

The theory described above assumes, as in most versions of spin-dependent density functional theory, that the electronic spin points in a global "up" or "down" direction, excluding the possibility that electrons on different atoms might be aligned in different directions. This is a difficult problem in density functional theory. A simplified approach valid within the Atomic Moment Approximation (AMA) was made by Pickett.[17] We have adapted[40] it to our tight-binding procedure (1-7) as follows:

For each atom, define the paramagnetic part of each on-site term as

$$t_{i\ell} = (h_{i\ell\uparrow} + h_{i\ell\downarrow})/2 \ , \tag{9}$$

where the $h_{i\ell(\uparrow,\downarrow)}$ are defined in (6). Define the exchange splitting introduced by the polarization by

$$\Delta_{i\ell} = (h_{i\ell\uparrow} - h_{i\ell\downarrow})/2 \ . \tag{10}$$

Note that both (9) and 10) define diagonal elements in the Slater-Koster Hamiltonian. To introduce non-collinear spin polarization, we give each atom a spin direction $\hat{d}_i$, where $|\hat{d}_i| = 1$. We then construct the non-orthogonal Slater-Koster Hamiltonian by coupling the majority and minority spin channels together. The hopping and overlap terms between majority and minority orbitals are assumed to be identical to the terms between orbitals of the same spin are have the form (7). The on-site terms, however, are mixed according to the rule

$$h_{i\ell s,j\ell' s'} = t_{i\ell}\,\delta_{i,j}\delta_{\ell,\ell'} - 1/2\,\Delta_{i\ell}\,\delta_{i,j}\delta_{\ell,\ell'}\,\hat{d}_i \cdot \vec{\sigma}_{ss'} \ , \tag{11}$$

where the s and s' components indicate the spin index ($\uparrow$ or $\downarrow$), and $\vec{\sigma}_{ss'}$ is the vector form of the Pauli spin matrices for spins s and s'.

The simplest application of non-collinear magnetization is an anti-ferromagnet, where the $\hat{d}_i$ are along the Cartesian directions $\hat{z}$ and $-\hat{z}$. This a common model for Chromium,[41] which has a nominally bcc structure modulated by an incommensurate spin-density wave with vector $\mathbf{q} = (2\pi/a)(0, 0, 0.952)$. If we model this vector by $(2\pi/a)(0, 0, 1)$, which is the ground state of all first-principles calculations using current Density Functionals,[42] then the wave is commensurate and we can model it as an antiferromagnetic CsCl-like unit cell with atoms on the Cesium sites having spins pointing in the $\hat{z}$ direction and atoms on the Chlorine sites point along the opposite direction. We computed the total energy for this

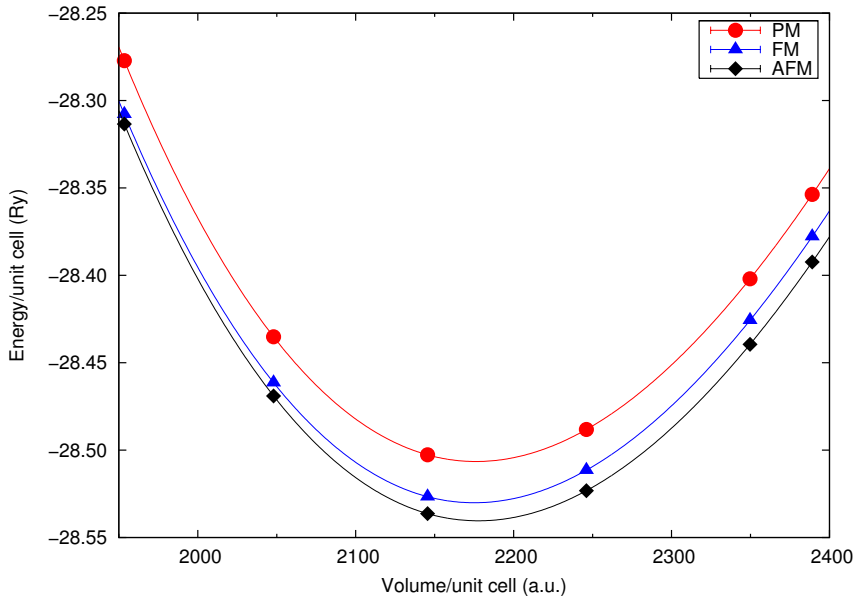

FIG. 4: Tight-binding total energy calculations for α-Manganese, using spin-polarized and unpolarized parameters and the non-collinear tight-binding method.[40] The paramagnetic (PM) calculations used the average of the spin-up and spin-down parameters. The ferromagnetic (FM) calculations used the spin-polarized parameters with all the atomic spins aligned. For nearly antiferromagnetic (AFM) calculations, atoms at the (2a) and one set of (24g) Wyckoff positions were aligned in the "up" direction, and atoms on the (8c) and second (24g) sites were aligned "down." This yields the lowest possible total spin for the primitive 29-atom α-Mn unit cell.

state by using our spin-polarized tight-binding parameters for Cr, and equations (9-11), alternating the "up" and "down" spins in a CsCl structure, to yield the results shown in Fig. 3. We see that the antiferromagnetic phase has lower energy than the ferromagnetic phase for all volumes, in agreement with experimental data.

Manganese is another element with an antiferromagnetic ground state. We have previously shown [43] that paramagnetic tight-binding parameters correctly predict the ground state αMn structure, but we did not consider the effects of magnetic interactions. Using a spin-polarized set of tight-binding parameters, fitted to the fcc, bcc, and simple cubic structures, we computed the total energy of αMn for all possible spin configurations which preserve the symmetry of the crystal. As shown in Fig. 4, we found that a configuration with 13 "up" atoms and 16 "down" atoms gives the lowest energy. Given the constraints of the 29-atom unit cell we cannot get a perfect antiferromagnet. This will require (at least)

doubling the unit cell.

An alternative method for determining magnetization within a parametrized tight-binding framework was developed by Mukherjee and Cohen.[44] In this method the net magnetic moment (8) is considered to be a parameter, and is solved for self-consistently. This allows ferromagnetic and paramagnetic systems to be computed from the same set of parameters. The method has been successfully applied to high pressure hcp Iron,[45] which has a rather unusual magnetic structure.[46], Zhuang and Halley[47] use a charge self-consistent tight-binding method to describe the non-collinear magnetic spin structures of MnF_2 and MnO_2.

II. COMPOUNDS

Extension of the method to compounds requires several modifications.[48] As always, we begin by shifting the eigenvalues so that their sum is the total energy

$$E[n(\mathbf{r})] = \sum_n f(\varepsilon'_n - \mu')\,\varepsilon'_n \ , \tag{12}$$

There are three types of parameters in the fit: the on-site terms, which depend on the local environment and represent the energy required to put an electron in a specific atomic shell, the hopping parameters, which represent the energy required for the electron to move between atoms, and overlap parameters, detailing the non-orthogonality of the tight-binding orbitals. In all three cases we must now determine pairwise interactions between atoms of the same type as well as those between atoms of different species.

The environmental dependence of the on-site parameters is controlled by a set of atomic-like densities,

$$\rho(i,\tilde{j}) = \sum_{j\in\tilde{j}} \exp[-\lambda^2_{\tilde{i}\tilde{j}}|\mathbf{R_i} - \mathbf{R}_j|]\mathcal{F}(|\mathbf{R}_i - \mathbf{R}_j|) \ , \tag{13}$$

where the i^{th} atom is of type $\tilde{i}$, the j^{th} atom is of type $\tilde{j}$, $\rho(i,\tilde{j})$ is the density on atom i due to atoms of type $\tilde{j}$, and $\lambda_{\tilde{i}\tilde{j}}$ is a fitting constant to be determined, and $\mathcal{F}$ is defined in (4).

The on-site terms themselves are polynomial functions in $\rho^{2/3}$:

$$h_\ell(i) = a_\ell(\tilde{i}) + \sum_{\tilde{j}}[b_\ell(\tilde{i},\tilde{j})\rho(i,\tilde{j})^{2/3} + c_\ell(\tilde{i},\tilde{j})\rho(i,\tilde{j})^{4/3} + d_\ell(\tilde{i},\tilde{j})\rho(i,\tilde{j})^2] \ , \tag{14}$$

where the sum is over all atom types in the system. Each atom type interacts with the target atom differently. The method used here was adopted for the sake of expediency, and is not

the ideal form. However, it is a very useful form, as we shall see. In general we use angular momenta $\ell = s, p, d$. However, in systems with essentially cubic symmetry it is sometimes convenient to split the d on-site terms into t_g and e_{2g} components. We took this approach for the parametrization of FeAl,[48] but not for Cu-Au.[49]

The two-center Slater-Koster hopping integrals are determined using an exponentially damped polynomial, and depend only on the atomic species and the distance between the atoms:

$$H_{\ell\ell'\mu}(i,j;R) = [A_{\ell\ell'\mu}(\tilde{\imath},\tilde{\jmath}) + B_{\ell\ell'\mu}(\tilde{\imath},\tilde{\jmath})R + C_{\ell\ell'\mu}(\tilde{\imath},\tilde{\jmath})R^2]\exp[-D^2_{\ell\ell'\mu}(\tilde{\imath},\tilde{\jmath})\,R]\mathcal{F}(R)\ . \qquad (15)$$

The A, B, C and D parameters are to be fit. For like-atom ($\tilde{\jmath} = \tilde{\imath}$) interactions, there are 10 independent Slater-Koster parameters:

$$ss\sigma, sp\sigma, pp\sigma, pp\pi, sd\sigma, pd\sigma, pd\pi, dd\sigma, dd\pi, \text{and } dd\delta\ .$$

When the atoms are of different types, we must include an additional four parameters,

$$ps\sigma, ds\sigma, dp\sigma, \text{and } dp\pi\ .$$

Note that we do not distinguish between t_g and e_{2g} orbitals when computing the hopping integrals.

Since we are using a non-orthogonal basis set, we must also parametrize the overlap integrals. These have a form similar to the hopping integrals:

$$S_{\ell\ell'\mu}(i,j;R) = [O_{\ell\ell'\mu}(\tilde{\imath},\tilde{\jmath}) + P_{\ell\ell'\mu}(\tilde{\imath},\tilde{\jmath})R + Q_{\ell\ell'\mu}(\tilde{\imath},\tilde{\jmath})R^2]\exp[-T^2_{\ell\ell'\mu}(\tilde{\imath},\tilde{\jmath})\,R]\mathcal{F}(R)\ , \qquad (16)$$

where O, P, Q and T also represent parameters to be fit. Again we do not distinguish between t_g and e_{2g} orbitals.

For a two-component system with s, p, d orbitals, including t_g and e_{2g} on-site terms, there are 330 parameters (λs, a, b, c, d, A, B, etc.) which are used in the fit, in contrast to 97 for a single-element parametrization.[10] These parameters are chosen so as to reproduce the eigenvalues ε' and energies E in equation (12). While the number of parameters may seem rather large, one must realize that we are using these parameters as a mathematical transformation from the DFT to the TB formalism. With this in mind, the number of parameters seems quite reasonable.

Copper-Gold

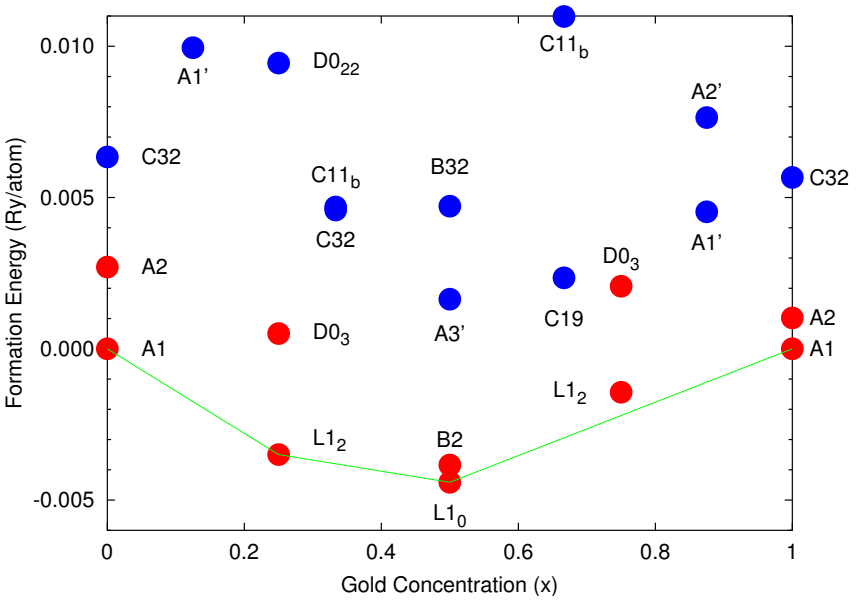

FIG. 5: Formation energy diagram for ordered $Cu_{1-x}Au_x$ compounds, using our tight-binding parameters.[6, 49] *Strukturbericht* symbols are used to designate the phases, except for A1' and A2', which are ordered Cu_7Au and $CuAu_7$ supercells of the fcc and bcc lattices, respectively. The tie line connects the known ordered structures in the Cu-Au system.[50] The red dots represent structures used to fit the tight-binding parameters, while the blue dots are predictions.

A good test case for the method is the Cu-Au system. Experimentally it is known that ordered phases exist up to 200-400 °C for Cu_3Au ($L1_2$), CuAu ($L1_0$), and $CuAu_3$ ($L1_2$).[50] Theoretically, Ozoliņš, Wolverton and Zunger[51] have done extensive first-principles calculations on hypothetical ordered phases in this system, using the energetics data to fit a cluster expansion model for the alloy. In our calculations, we first obtained good tight-binding parameters for Cu[52] and Au.[12] These were fixed throughout the remainder of the fit. We then fit the Cu-Au on-site, hopping, and overlap terms to reproduce the band structure and total energies of Cu_3Au and $CuAu_3$ in the $L1_2$ and $D0_3$ structures, and CuAu in the $L1_0$, $L1_1$, B1, and B2 structures. We then compute the total energies of a number of ordered structures, and compute the formation energy per atom, which, for a structure with formula unit Cu_mAu_n is

$$E_{\rm form}(m,n) = [E_0(Cu_mAu_n) - nE_{\rm fcc}(Cu) - mE_{\rm fcc}(Au)]/(m+n)\ . \qquad (17)$$

where E_0 is the minimum energy for the structure in question, and $E_{\rm fcc}$ is the equilibrium energy of the pure element in the face-centered cubic phase. The results for the low-lying

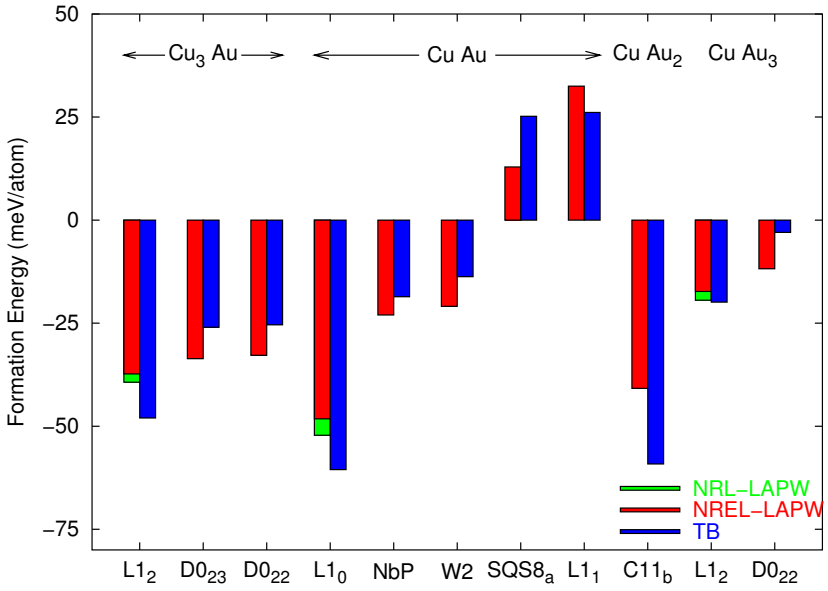

FIG. 6: Formation energy of several ordered phases in the Cu_xAu_{1-x} system, calculated using our tight-binding parameters[6, 49] (blue bars), and compared to first-principles calculations performed by Ozoliņš *et al.*[51] (red bars). The structure notation is from Ref. [51]. On this scale, the cluster-expansion energies found in Ref. [51] are indistinguishable from the corresponding LAPW results. For comparison, we also plot our first-principles LAPW results (green bars), which were used in the Cu-Au tight-binding fitting process.

phases in the Cu-Au system are shown in Fig. 5. We see that these parameters do, in fact, predict the existence of ordered $L1_2$ Cu_3Au and $L1_0$ CuAu. The $L1_2$ $CuAu_3$ structure is, on the other hand, above the tie-line between CuAu and pure gold. This is consistent with our LAPW calculations, suggesting that $L1_2$ is not the ground state structure of $CuAu_3$.

Figure 6 compares some of our structural energies to the first-principles formation energies found by Ozoliņš *et al.*[51] We see that we have very good agreement for the low-lying phases. Part of the discrepancy may be that we disagree slightly on the first-principles formation energies of some structures, as shown in the figure.

To further assess the transferability of the Cu-Au parameters, we computed elastic constants and zone-center phonon frequencies for ordered Cu_3Au and compared them to experiment[53, 54] as well as first-principles LAPW calculations. The results are shown in Table III. We find reasonable agreement between these values and results obtained from first-principles.

TABLE III: Equilibrium bulk properties of Cu_3Au in the $L1_2$ structure, as determined by our tight-binding parametrization[49], first-principles LAPW calculations, and from experiment.

Property	Experiment	LAPW	TB
a (Å)	3.755[53]	3.68	3.69
C_{11} (GPa)	187[30]	180	198
C_{12} (GPa)	135[30]	120	98
C_{44} (GPa)	68[30]		92
Γ_4 (cm^{-1})	125[54]	110	153
Γ_4 (cm^{-1})	210[54]	200	270
Γ_5 (cm^{-1})	161[54]	159	195

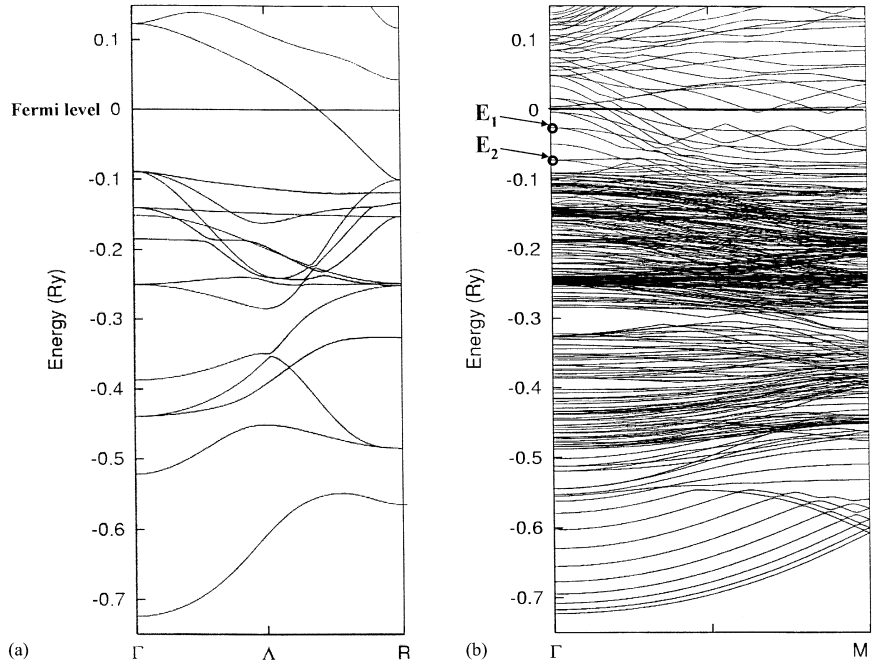

FIG. 7: Band structure of the Cu_3Au from [49]: (a) bulk system along the ΓR direction, and (b) (111) surface along the ΓM direction. E_1 and E_2 are the experimentally determined surface states.[55]

The advantage of the tight-binding method over first-principles is that it allows us to quickly study systems with a large number of atoms. Accordingly, we used these parameters to seek understanding of the surface electronic structure of Cu_3Au.[49] Experiment[55] shows that two electronic surface states exist at $\overline{\Gamma}$ in the (111) surface Brillouin zone of Cu_3Au.

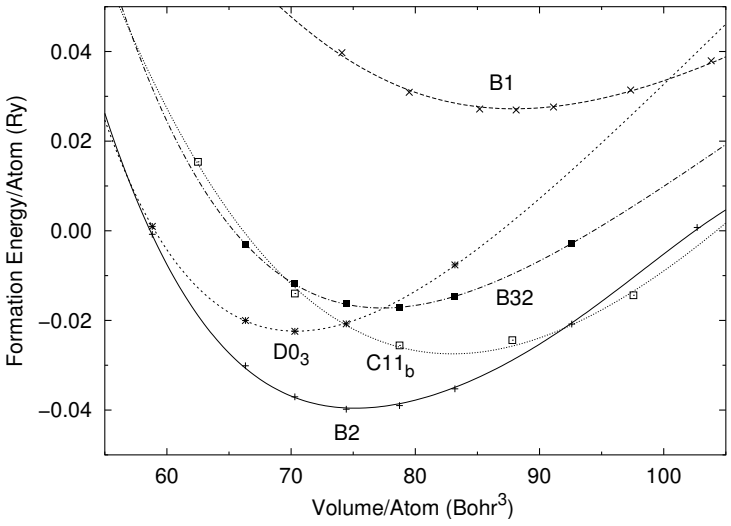

FIG. 8: The formation energies versus atomic volume for ordered Fe_xAl_{1-x} structures, calculated using our TB parameters[48] and compared to first-principles LAPW calculations. The solid lines represent the TB results while the points represent the LAPW results.

We model this system using our TB parameters and a slab consisting of 15 atomic layers and 60 atoms. In Fig. 7, we compare band structures for bulk Cu_3Au and the slab. We see that the surface states found experimentally agree nicely with the states found in our TB calculation.

Aluminides, Hydrides, and Carbides

To study aluminides we created a database of LAPW calculations for the B1 (NaCl), B2 (CsCl), D03 (Fe_3Al), $C11_b$ ($MoSi_2$), and B32 (NaTl) structures, generating TB Hamiltonians for FeAl,[48] CoAl, and NiAl by fitting the energy bands for the B2 structure and the total energies for all the above structures. The TB Hamiltonian included the s,p, and d orbitals for both the metal and Al sites, which were all necessary for obtaining a good fit to the LAPW results. The RMS error for the total energy was less than 1 mRy for all structures fitted, and in the B2 structure the RMS error for the lowest 12 bands was less than 20 mRy. We were able to reproduce well the lattice constants and bulk moduli, and electronic properties, such as the densities of states and energy bands. In addition, quantities that were not fitted, such as elastic constants, are found to be in good agreement with independent LAPW calculations and experiment.

Fig. 8 shows that there is excellent agreement between the LAPW results and the TB

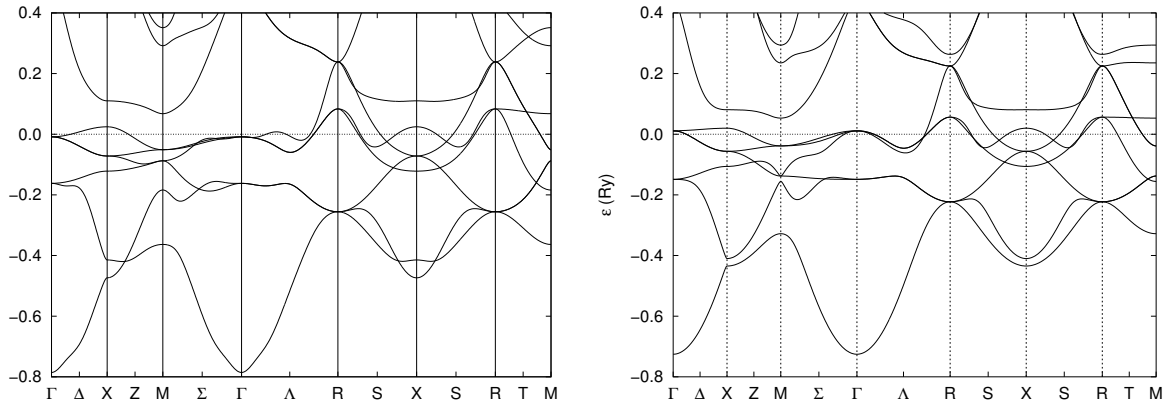

FIG. 9: The band structure of FeAl in the CsCl structure, at the lattice constant $a = 2.94$Å. The left figure shows the tight-binding band structure, while the LAPW results are on the right. In both cases the Fermi level has been set to zero. These calculations were done using a tight-binding parameter set which was selected to improve the fit to the FeAl band structure compared to our original parameters.[48]

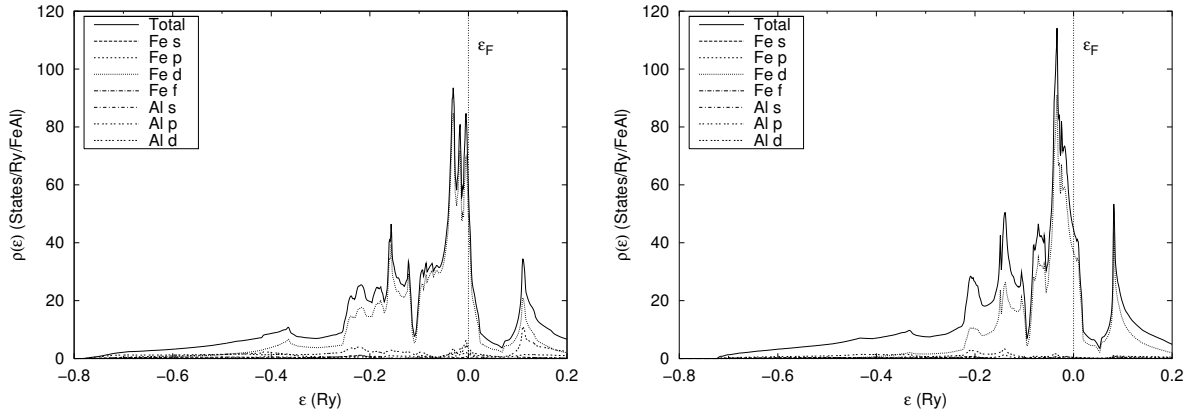

FIG. 10: The electronic density of states of B2 (CsCl) FeAl, using the TB (left) and LAPW (right) methods, at the lattice constant $a = 2.94$Å. In each case the Fermi level has been set to zero. The partial densities of states are given according to the legend in each part of the figure. While the LAPW results have a longer tale at low energy, the DOS are essentially similar near the Fermi level.

results over a wide range of pressures for all the fitted phases. The agreement is especially good in the ground-state CsCl (B2) structure. We plot the formation energy, which is defined in analogy with (17).

The TB and LAPW band structures of the B2 FeAl structure are shown in Fig. 9. The

original TB calculations[48] reproduces the main features of the first-principles results, but in detail there are significant differences. Here we use a parameter set which has a better fit to the band structure, and find that the behavior of the bands near the Fermi level is close to the LAPW results. We obtained the TB and LAPW electronic densities of states (DOS) by the tetrahedron method,[56] using 165 k-points in the irreducible part of the Brillouin zone. The LAPW and TB DOS shown in Fig. 10 are in good agreement. Experimentally, the DOS at the Fermi energy is known only from specific-heat measurements, where it was measured to be $\rho(\varepsilon_F)$ = 31.1 states/Ry/FeAl molecule.[57] Our TB calculation yields (F) = 48.7 states/Ry, slightly higher than the LAPW value $\rho(\varepsilon_F) = 36.8$. Other reports in the literature also find the theoretical value of $\rho(\varepsilon_F)$ to be greater than that from experiment, a discrepancy that does not allow for electron-phonon enhancement, which puts the experimental result into question. This discrepancy is possibly caused by the non-stoichiometry of the Fe-Al samples.

Our predicted equilibrium lattice parameters and bulk modulus are also in good agreement with the first-principles results shown in Table IV. This is a result of the fitting procedure, as we fit the TB parameters to total energies at several volumes. However, the shear elastic moduli that we computed[29, 58] for the CsCl phase were not included in the fit, and except for C_{44} are in good agreement with the experimental results. In summary, we have presented a brief report of our TB study of the FeAl system. We showed that the parameters describe excellently several bcc and bcc-like phases as well as the NaCl phases.

We have also developed tight-binding parametrizations for several other binary compounds. We can judge the transferability of the parameters by computing elastic constants for the equilibrium phase and comparing to experiment, as we do in Table IV. In many cases, the compound measured is not stoichiometric, e.g., $PdH_{0.66}$[59] or $Fe_{0.5989}Al_{0.4011}$[30], or only has been measured in thin films.[60] In extreme cases, where there is no available experimental data, we compare to the results of LAPW calculations.[58]

The tight-binding method described here is not limited to the study of bulk systems. It can, indeed, be used to study chemisorption processes. Our initial work was on the Pd-H_2 system. [63] Building on our previous parameters for Pd,[9] and using a database of 55 *ab initio* total energy calculations, we were able to model dissociation of molecular hydrogen at the Pd (100) surface. We modified our usual procedure so that the fitting was done varying only the hydrogen on-site terms and the H-H and Pd-H Hamiltonian and overlap hopping

TABLE IV: Equilibrium lattice parameters and elastic constants (in GPa) for various cubic compounds in the NaCl or CsCl structure. Tight-Binding results are compared to the available experimental data, noting that some compounds do not exist at the given stoichiometry. Values are calculated at the indicated equilibrium lattice constants (in atomic units).

	NiH		PdH		FeAl		NiAl		CoAl		NbC		VN	
	TB	LAPW	TB	Exp.[59]	TB	Exp.[30]	TB	Exp.[30]	TB	LAPW[58]	TB	Exp.[61]	TB	Exp.[6
a	6.908	6.908	7.723	7.584	5.323	5.479	5.389	5.461	5.295	5.408	8.405	8.447	7.873	7.810[6
B	238	234	207	183	204	136	195	166	213	157	313	340	333	2
C_{11}	353	311	282	227	313	181	247	211	306	257	639	620	570	5
C_{12}	181	196	170	161	149	114	168	143	166	107	151	200	214	1
C_{44}	92	64	27	69	71	127	60	112	82	130	126	150	170	1

parameters. The Pd on-site terms and Pd-Pd parameters were kept fixed to their pure Pd values. However, to obtain higher accuracy we expanded the polynomial that described the H-H and Pd-H parameters up to fourth order.

Figure 11 shows potential energy surface cross-sections for two orientations of the H_2 molecule above the surface. A comparison of the TB and *ab initio* results reveals that the fit reproduces the minimum energy paths and also the general shape of the elbow plots very well. The overall RMS error, including additional ab initio values that were not fitted, was only 0.1 eV, a value that is usually considered to be within the accuracy of the *ab initio* total energies.

Using similar techniques, we have also developed a set of tight-binding parameters for studying the dissociation of the O_2 molecule as it approaches a platinum surface.[64] In addition to the energy surfaces (as we computed for Pd-H_2), we used the Tight-Binding Molecular Dynamics (TBMD)[12] code to compute sticking probabilities. This was done by performing TBMD runs for a number of incident O_2 kinetic energies in the range 0-1.5 eV, and averaging over 150 trajectories for a given energy. The results are shown in Fig. 12. We see that the trapping probability has the same basic behavior as found experimentally,[65, 66] showing that we can successfully model the chemisorption of O_2 on Pt.

Silicon Carbide

We previously developed parameter sets for both Carbon[67] and Silicon,[68] so it is natu-

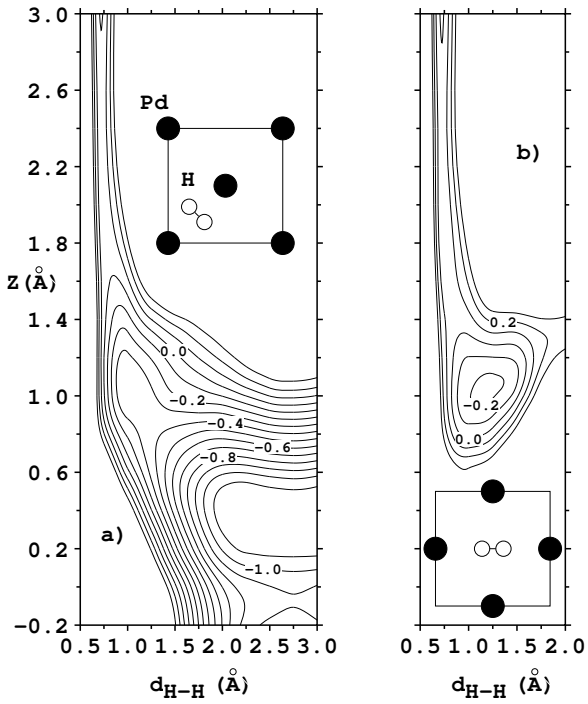

FIG. 11: Contour plots of the TB-PES along two two-dimensional cuts through the six-dimensional coordinate space of H_2/Pd(100).[63] The coordinates in the figure are the H_2 center-of-mass distance from the surface Z and the H-H interatomic distance d_{H-H}. The lateral H_2 center-of-mass coordinates in the surface unit cell and the orientation of the molecular axis, i.e., the coordinates X, Y, u, and f are kept fixed for each 2D cut and depicted in the insets. The molecular axis is kept parallel to the surface; (a) corresponds to the dissociation at the bridge site, (b) to dissociation at the top site. The dots denote the points that have been used to obtain the fit. Energies are in eV per H_2 molecule. The contour spacing is 0.1 eV.

ral to extend the technique to the development of a parameter set for SiC.[69] Silicon carbide has a wide variety of polytypes, distinguished by the stacking of the SiC layers. It is therefore a good test of the ability of the method to develop transferable parameter sets. The parameters were developed by fitting to the zincblende (stacking ABCABC), wurtzite (stacking ABAB), and 4H (stacking ABACABAC) structures, several zone-boundary phonons, elastic constant modes, and diamond Si and C. The method was able to successfully reproduce the first-principles electronic band structure, as shown in Fig. 13. In addition, we computed phonon frequencies along the (001) direction of the zincblende unit cell and compared them

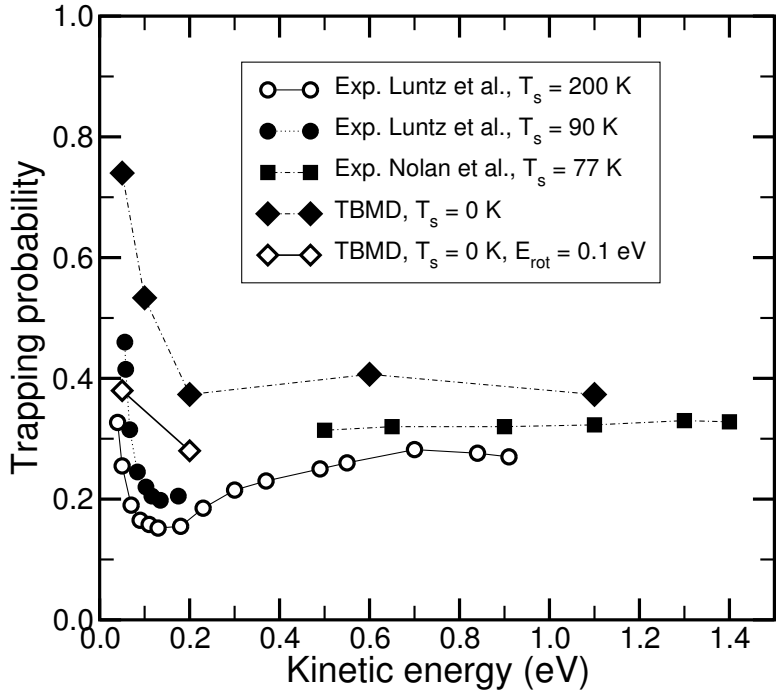

FIG. 12: Trapping probability of O_2/Pt(111) as a function of the kinetic energy for normal incidence. [64] Results of molecular beam experiments for surface temperatures of 90 and 200 K[65] and 77 K[66] are compared to TBMD simulations for the surface initially at rest ($T_s = 0$ K).

to experiment.[70] As seen in Fig. 14, the acoustic modes are in good agreement with experiment, though the optic modes are somewhat low. Thermal expansion was also computed using the TBMD program, and found to be in good agreement with experiment.

Tight-binding description of MgB_2

A nonorthogonal TB Hamiltonian for the superconductor MgB_2 was derived[71] by fitting to both the total-energy and energy-band results of a first-principles full-potential LAPW calculation using the Hedin-Lundqvist parametrization of the local-density approximation LDA. The LAPW calculations were performed in the ground-state (AlB_2) structure, for 17 different combinations of c and a, that determined the LDA equilibrium volume. The LAPW results for the total energy and the energy bands at 76 k points in the irreducible hexagonal Brillouin zone, were used as a database to determine the parameters of the TB Hamiltonian. Our basis included the s and p orbitals in both Mg and B in a nonorthogonal two-center representation. In order to obtain an accurate fit it was essential to block diagonalize the Hamiltonian at the high-symmetry points Γ, A, L, K, and H. We found that at a given set of lattice parameters (c,a) we can reproduce the energy bands of MgB_2 quite well. A

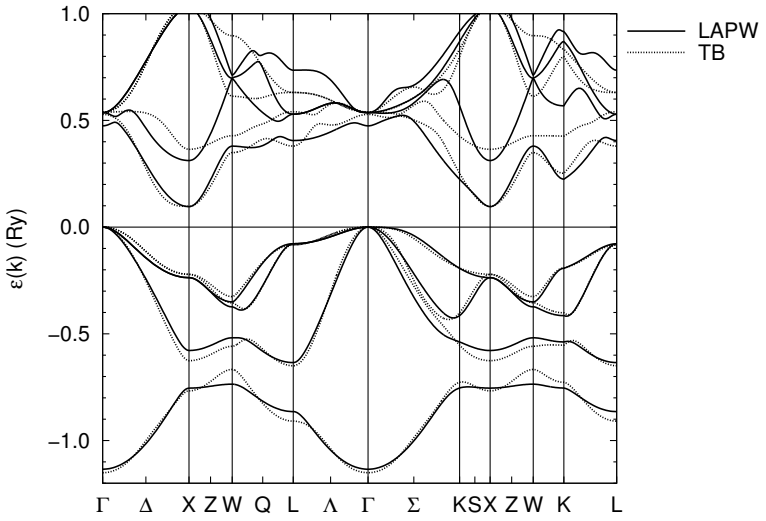

FIG. 13: Band structure of zincblende SiC along high symmetry directions of the Brillouin zone, calculated from sp^3d^5 tight-binding parameters (solid lines) and LAPW-LDA (dashed lines).[69]

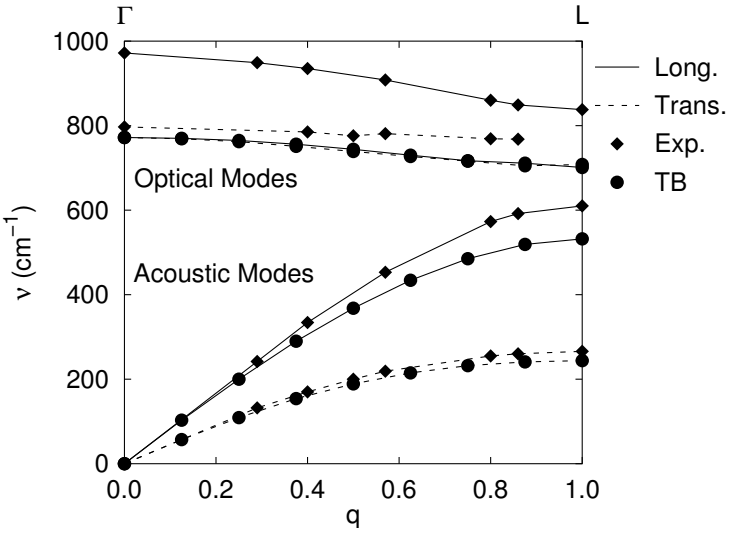

FIG. 14: Phonon dispersion along the $\Gamma - L$ direction in zincblende SiC. Circles are from an sp^3 tight-binding parametrization,[69], and diamonds are from experiment.[70]

comparison is shown in Fig. 15, where the solid and broken lines represent the LAPW and TB bands, respectively, at the LDA values of the equilibrium lattice parameters. The TB bands are in very good agreement with the LAPW bands, including the two-dimensional B- band in the A direction just above , which has been identified as hole-band-controlling superconductivity. The RMS fitting error is 2 mRy for the total energy, and close to 10

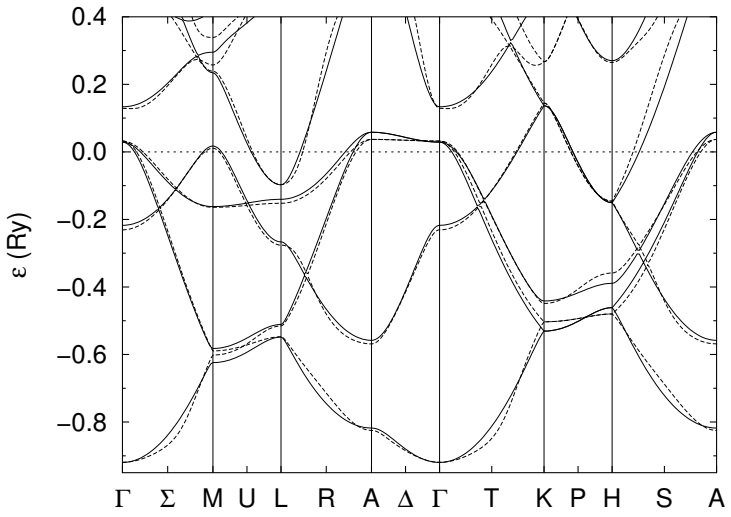

FIG. 15: The band structure of MgB_2 in the AlB_2 structure at the theoretical equilibrium volume, as determined by the full-potential LAPW method (solid lines) and our tight-binding parametrization dashed lines.[71] The Fermi level is at zero.

mRy for the first five bands. Beyond the fifth band our fit is not as accurate, as the Mg d bands, which are not included in our Hamiltonian, come into play. The values of our TB parameters are given in the references.[71] In Fig. 16 we show a comparison of TB and LAPW densities of states DOS. There is an excellent agreement in both the total DOS and the B p-like DOS.

The B and Mg s components of the DOS have their strongest presence at the bottom of the valence band, from -0.8 Ry to -0.6 Ry on our scale. They are much smaller than the p-like DOS, so we chose not to include them in Fig. 16. Additionally, we have omitted the Mg p-like DOS, which is also small below ε_F, but becomes significant above E_f. Our TB value of the total DOS at ε_F is $\rho(\varepsilon_F) = 0.69$ states/eV, which is almost identical to that found from our direct LAPW calculation. This value of $\rho(\varepsilon_F)$ corresponds to the LDA equilibrium volume and is slightly smaller than the value of 0.71 states/eV reported by other workers at the experimental volume. Using our value of $\rho(\varepsilon_F)$ and the measured value of the specific-heat coefficient γ we find a value of the electron-phonon coupling constant $\lambda = 0.65$, which is consistent with the high superconducting-transition temperature in MgB_2.

Our TB Hamiltonian also provides an accurate description of the energetics of MgB_2, as shown in Fig. 17. We have tested our parameters by computing the TB equilibrium

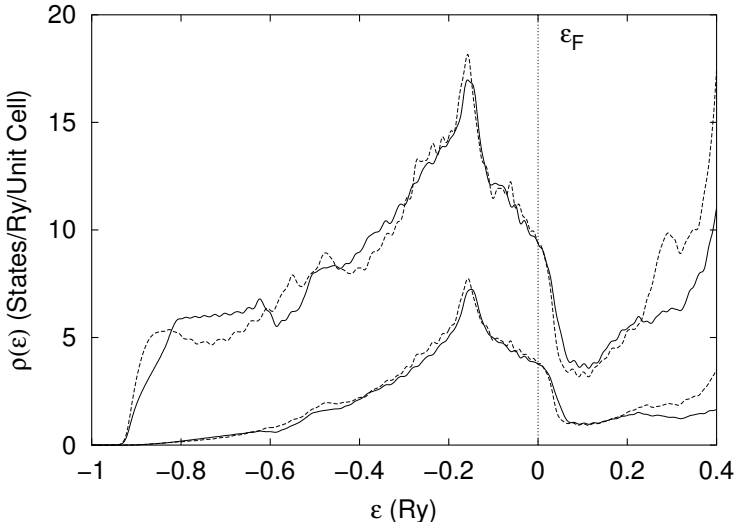

FIG. 16: The electronic density of states DOS of MgB_2 in the AlB_2 structure at the theoretical equilibrium volume, comparing the total DOS as determined by the full-potential LAPW method (upper solid line) and our tight-binding parametrization[71] (upper dashed line), and the partial single-atom B p decomposition lower lines.

structure. We find an equilibrium of c 6.66 a.u. and a 5.79 a.u., in good agreement with the LAPW result. At c/a = 1.14 ,the experimental value, we deduce a bulk modulus of B = 165 GPa which is in good agreement with the experimental value of 120 GPa and with the calculated value of 147 GPa reported by Bohnen *et al.*[72]

Ternary systems: Ruthenates

The NRL-TB scheme has been applied to ternary systems as well. For such applications the number of parameters increases substantially. However, in most cases it is easy to restrict the number of parameters by using an orthogonal Hamiltonian and by reducing the orbitals to only those who are the most dominant in the particular system. We consider first[73] $SrRuO_3$ and Sr_2RuO_4 where for the former we have constructed a 14x14 orthogonal Hamiltonian including Ru-d and O-p orbitals and for the latter the Hamiltonian size is 27x27 with Sr-d, Ru-d, and O-p orbitals. In these calculations we did not fit the total energies, as we aim only for a very accurate reproduction of the LAPW band structures. These Hamiltonians allow the band structure to be computed on very fine meshes in the Brillouin zone at low computational cost, and additionally have yielded an analytic form for band velocities, while retaining the accuracy of the full-potential electronic structure calculations.

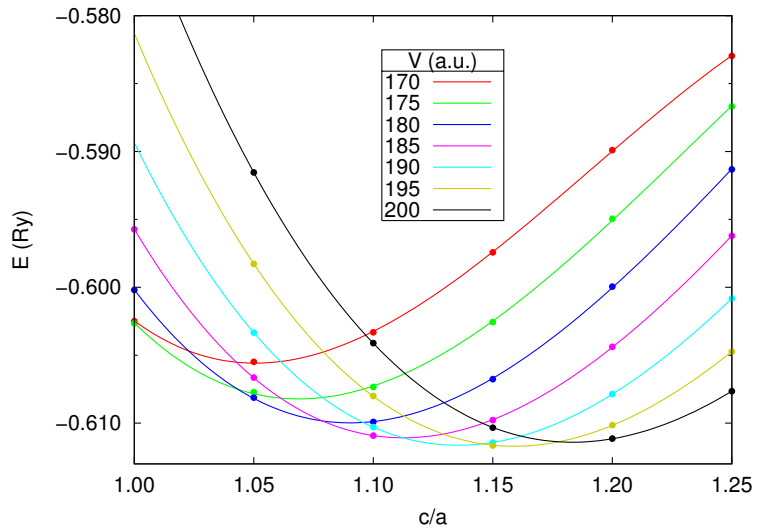

FIG. 17: Total energy of MgB_2, at fixed volume versus c/a, calculated from our tight-binding parametrization.[71] The points indicate the actual calculated energies, while the lines are cubic polynomial fits to the data.

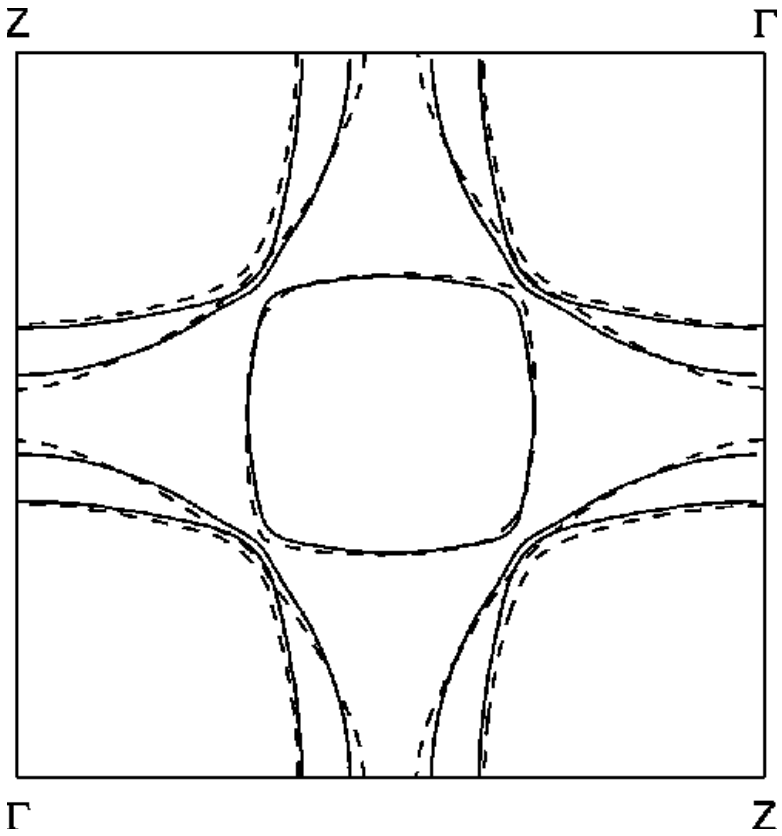

FIG. 18: Fermi surface of $SrRuO_4$ from LAPW and TB calculations.[73]

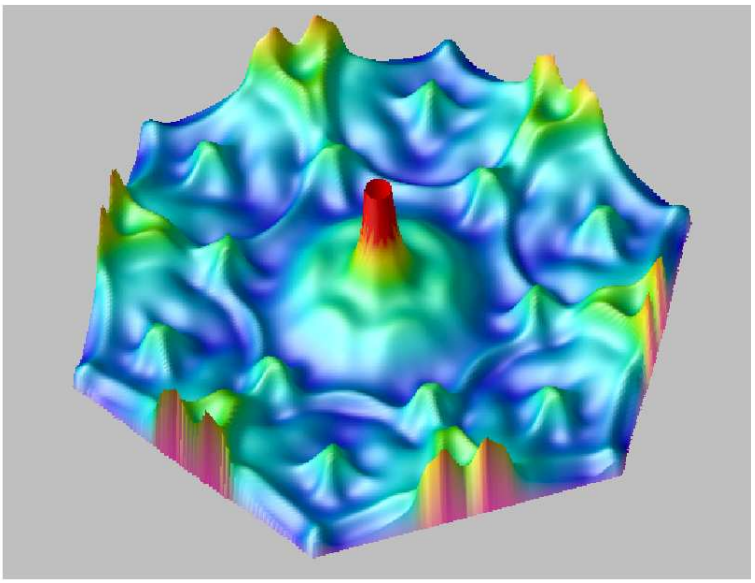

FIG. 19: Low frequency limit of $\chi_0''(\mathbf{q},\omega)/\omega$ in Na_xCoO_2, using a tight-binding parametrization of Co-O,[74] The double humped peaks on the zone boundary indicate nesting.

This greatly facilitates calculation of transport and superconducting parameters related to the fermiology. These features were exploited to calculate the Hall coefficient and an anisotropy parameter relevant to the superconducting vortex lattice geometry for Sr_2RuO_4.

A comparison of TB and LAPW Fermi surface for Sr_2RuO_4 is shown in Fig. 18 where we see an excellent agreement.

Na_xCoO_2

The TB method has been applied to the study of the odd-gap superconductor Na_xCoO_2.[74, 75] This system has strong nesting, involving nearly 70% of the electrons at the Fermi level. Since this effect primarily involves the Co and O atoms, the parametrization was restricted to those states. The crystal field of the octahedral structure splits the on-site Co d-bands into a_{1g}, e_g, and e_g' bands. To accommodate this, the on-site parameters (14) were computed independently for the xy, yz, zx, x^2-y^2, and $3z^2-r^2$ Co d orbitals and the x, y, and z O p orbitals. The dependence of the on-site and hopping parameters on bond distance was then used to analyze the Fermi surface change with interlayer distance. The band structure and Fermi surface was found to depend on the Oxygen height in a non-trivial manner. In addition, the one-electron susceptibility was then computed, as shown in Fig. 19. The nesting shown hear leads to a charge density wave as well as spin-fluctuations,

suggesting that system is an odd-gap triplet s-wave superconductor.

Other methods

Porezag, *et al.*[8] developed an alternative method for computing total energies and electronic eigenvalues from a parametrized tight-binding scheme. In their work, based on the Linear Combination of Atomic Orbitals (LCAO) method, the hopping parameters computed directly from first principles calculations. A repulsive pair potential between the ions is then fitted so that the sum of the pair potential energies and the sum over the occupied states gives the correct total energy. Finally, the on-site terms are corrected with a simulated Coulomb interaction to preserve charge self-consistency on each ion. The method has been applied to many sp^3 systems, including *e.g.*, predicting the structure of tetragonal CN compounds,[76] the electronic structure of GaN edge dislocations, and the structure of amorphous CN.[77]

Halley and co-workers[7, 78, 79] have developed a similar charge self-consistent tight-binding approach, which has been applied mainly to oxides (rutile TiO_2) and fluorides (MnF_2, discussed in Sec. I). In this method the isolated ions are required to have the proper energy levels, which allows for better descriptions of electrochemistry. As noted above, this method has also been used to study magnetic systems.

Pan[80] adapted the work of the Ames group on carbon[11] to derive a tight-binding parametrization for hydrocarbons. This has been used to study the geometries of small hydrocarbons and hydrogenated diamond surfaces, and finds geometries in qualitative agreement with previous results.

We have discussed extensions of the our original tight-binding total energy method[9, 10] to spin-polarized systems, including non-collinear spins, and compounds. Although the determination of the TB parameters is tedious, the resulting method is computationally efficient, capable of performing static and dynamic calculations beyond the limits of first-principles methods. We have applied the method to all of the magnetic elements, and many non-magnetic compounds. The accuracy of electronic, elastic, and phonon properties is comparable to that of the original, non-magnetic single element calculations.

III. OUTLOOK

Tight-binding total energy methods can be thought of as a mapping of a large set of first-principles data onto a compact TB Hamiltonian based on Slater-Koster parameters.

As we have seen, these methods are nearly as accurate as first-principles calculations over a wide range of structures and densities. The calculations are very fast, as well. A typical first-principles calculation for a transition metal or intermetallic compound requires on the order of one hundred basis functions per atom to achieve convergence. The TB calculation will use only nine functions per atom, assuming an sp^3d^5 basis set. Given that the time to diagonalize Hamiltonian scales as the cube of the number of basis functions, we see that TB methods are inherently one thousand times faster than the corresponding first-principles calculations. Furthermore, any algorithmic improvements in eigenvalue determination can be applied to TB methods as well as first-principles. Tight-binding calculations will therefore always be faster than first-principles, and so can be applied to much larger systems. As we have seen, these methods are routinely applied to molecular dynamics simulations containing hundreds of atoms, and have been applied to systems containing several thousand atoms.

The major bottleneck to the widespread use of TB methods is the development of accurate parameter sets, particularly for binary and ternary compounds. This involves large numbers of first-principles calculations, and thorough testing of the resulting parameter sets. However, once a parameter set is validated, it can be used for a wide variety of applications. We expect the use of TB methods to grow rapidly as more systems are parametrized.

Acknowledgments

This work was supported by the U. S. Office of Naval Research (ONR). The development of the tight-binding codes was supported in part by the U. S. Department of Defense Common HPC Software Support Initiative (CHSSI). Work on the magnetic elements was sponsored in part by the ONR Design of Naval Steels program.

In addition to our collaborators, we would like to thank W. Pickett for helpful discussions concerning non-collinear magnetization.

Michael J. Mehl
(mehl@dave.nrl.navy.mil) and
D. A. Papaconstantopoulos
(papacon@dave.nrl.navy.mil)
Center for Computational Materials Science
Naval Research Laboratory
Washington, D.C. 20375-5000
United States

---

[1] J. C. Slater and G. F. Koster, Phys. Rev. **94**, 1498 (1954).

[2] W. A. Harrison, *Electronic Structure and the Properties of Solids* (Freeman, San Francisco, 1980).

[3] W. A. Harrison, *Elementary Electronic Structure* (World Scientific, Singapore, 1999).

[4] D. A. Papaconstantopoulos, *Handbook of the Band Structure of Elemental Solids* (Plenum, New York, 1986).

[5] M. J. Mehl and D. A. Papaconstantopoulos, in *Topics in Computational Materials Science*, edited by C. Y. Fong (World Scientific, Singapore, 1998), Chap. V, pp. 169–213.

[6] D. A. Papaconstantopoulos and M. J. Mehl, J. Phys.: Condens. Matt. **15**, R413 (2003).

[7] N. Yu and J. W. Halley, Phys. Rev. B **51**, 4768 (1995).

[8] D. Porezag, T. Frauenheim, T. Köhler, G. Seifert, and R. Kaschner, Phys. Rev. B **51**, 12947 (1995).

[9] R. E. Cohen, M. J. Mehl, and D. A. Papaconstantopoulos, Phys. Rev. B **50**, 14694 (1994).

[10] M. J. Mehl and D. A. Papaconstantopoulos, Phys. Rev. B **54**, 4519 (1996).

[11] M. S. Tang, C. Z. Wang, C. T. Chan, and K. M. Ho, Phys. Rev. B **53**, 979 (1996).

[12] F. Kirchhoff, M. J. Mehl, N. I. Papanicolaou, D. A. Papaconstantopoulos, and F. S. Khan, Phys. Rev. B **63**, 195101 (2001).

[13] H. Haas, C. Z. Wang, M. Fähnle, C. Elsässer, and K. M. Ho, Phys. Rev. B **57**, 1461 (1998).

[14] C. Z. Wang, B. C. Pan, and K. M. Ho, J. Phys.: Condens. Matt. **11**, 2043 (1999).

[15] R. E. Cohen, L. Stixrude, and E. Wasserman, Phys. Rev. B **56**, 8575 (1997), *erratum* Phys. Rev. B **58**, 5873 (1998).

[16] J. L. Mercer, Jr. and M. Y. Chou, Phys. Rev. B **49**, 8506 (1994).

[17] W. E. Pickett, J. Korean Phys. Soc. (Proc. Suppl.) **29**, S70 (1996).

[18] O. K. Andersen, Phys. Rev. B **12**, 3060 (1975).

[19] S.-H. Wei and H. Krakauer, Phys. Rev. Lett. **55**, 1200 (1985).

[20] D. Singh, Phys. Rev. B **43**, 6388 (1991).

[21] P. Hohenberg and W. Kohn, Phys. Rev. **136**, B864 (1964).

[22] W. Kohn and L. J. Sham, Phys. Rev. **140**, A1133 (1965).

[23] L. Hedin and B. I. Lundqvist, Journal of Physics C: Solid State Physics **4**, 2064 (1971).

[24] J. P. Perdew, J. A. Chevary, S. H. Vosko, K. A. Jackson, M. R. Pederson, D. J. Singh, and C. Fiolhais, Phys. Rev. B **46**, 6671 (1992).

[25] M. J. Gillan, J. Phys.: Condens. Matt. **1**, 689 (1989).

[26] N. C. Bacalis, D. A. Papaconstantopoulos, M. J. Mehl, and M. Lach-hab, Physica B: Condensed Matter **296**, 125 (2001).

[27] P. Entel, R. Meyer, K. Kadau, H. Herper, and E. Hoffmann, Eur. Phys. J. B **5**, 379 (1998).

[28] M. J. Mehl, Phys. Rev. B **47**, 2493 (1993).

[29] M. J. Mehl, B. M. Klein, and D. A. Papaconstantopoulos, in *Intermetallic Compounds - Principles and Practice*, edited by J. H. Westbrook and R. L. Fleischer (John Wiley and Sons, London, 1994), Vol. 1, Chap. 9, pp. 195–210.

[30] G. Simmons and H. Wang, *Single Crystal Elastic Constants and Calculated Aggregate Properties: A HANDBOOK*, 2^{nd} ed. (M.I.T. Press, Cambridge, Massachusetts and London, 1971).

[31] V. J. M. G. Shirane and R. Nathans, Phys. Rev. **162**, 528 (1967).

[32] R. J. Birgeneau, J. Cordes, G. Dolling, and A. D. B. Woods, Phys. Rev. **136**, A1359 (1964).

[33] S. C. Miller and W. F. Love, *Tables of irreducible representations of space groups and co-representations of magnetic space groups* (Pruett, Bolder, 1967).

[34] C. Barreteau, R. Guirado-López, M. C. Desjonquères, D. Spanjaard, and A. M. Oleś, Comp. Mat. Sci. **17**, 211 (2000).

[35] C. Barreteau, D. Spanjaard, and M. C. Desjonquères, Phys. Rev. B **58**, 9721 (1998).

[36] C. Barreteau, R. Guirado-López, D. Spanjaard, M. C. Desjonquères, and A. M. Oles, Phys. Rev. B **61**, 7781 (2000).

[37] C. Barreteau, M.-C. Desjonqueres, A. M. Oles, and D. Spanjaard, Phys. Rev. B **69**, 064432 (2004).

[38] Y. Xie and J. A. Blackman, Phys. Rev. B **66**, 085410 (2002).

[39] G. L. Krasko, J. Appl. Phys. **79**, 4682 (1996).

[40] M. J. Mehl, D. A. Papaconstantopoulos, I. I. Mazin, N. C. Bacalis, and W. E. Pickett, J. Appl. Phys. **89**, 6880 (2001).

[41] K. Hirai, J. Phys. Soc. Japan **67**, 1776 (1998).

[42] R. Hafner, D. Spisak, R. Lorenz, and J. Hafner, Phys. Rev. B **65**, 184432 (2002).

[43] M. J. Mehl and D. A. Papaconstantopoulos, Europhys. Lett. **31**, 537 (1995).

[44] S. Mukherjee and R. E. Cohen, J. Comp.-Aid. Mat. Des. **8**, 107 (2001).

[45] R. E. Cohen and S. Mukherjee, Phys. Earth Planet. Int. **143-144**, 445 (2004).

[46] G. Steinle-Neumann, L. Stixrude, and R. E. Cohen, PNAS **101**, 33 (2004).

[47] M. Zhuang and J. W. Halley, Phys. Rev. B **64**, 024413 (2001).

[48] S. H. Yang, M. J. Mehl, D. A. Papaconstantopoulos, and M. B. Scott, J. Phys.: Condens. Matt. **14**, 1895 (2002).

[49] C. E. Lekka, N. Bernstein, M. J. Mehl, and D. A. Papaconstantopoulos, Appl. Surf. Sci. **219**, 158 (2003).

[50] *Binary Alloy Phase Diagrams*, edited by T. B. Massalski (American Society for Metals, Metals Park, Ohio, 1987).

[51] V. Ozoliņš, C. Wolverton, and A. Zunger, Phys. Rev. B **57**, 6427 (1998).

[52] Y. Mishin, M. J. Mehl, D. A. Papaconstantopoulos, A. F. Voter, and J. D. Kress, Phys. Rev. B **63**, 224106 (2001).

[53] P. D. Bogdanoff, B. Fultz, and S. Rosenkranz, Phys. Rev. B **60**, 3976 (1999).

[54] S. Katano, M. Iizumi, and Y. Noda, J. Phys. F **18**, 2195 (1988).

[55] R. Courths, M. Lau, T. Scheunemann, H. Gollisch, and R. Feder, Phys. Rev. B **63**, 195110 (2001).

[56] O. Jepsen and O. K. Andersen, Solid State Communications **9**, 1763 (1971).

[57] H. Okamoto and P. A. Beck, Monatshefte für Chemie **103**, 907 (1972).

[58] M. J. Mehl, J. E. Osburn, D. A. Papaconstantopoulos, and B. M. Klein, Phys. Rev. B **41**, 10311 (1990), *erratum* Phys. Rev. B **42**, 5362 (1990).

[59] D. K. Hsu and R. G. Leisure, Phys. Rev. B **20**, 1339 (1979).

[60] J. O. Kim, J. D. Achenbach, P. B. Mirkarimi, M. Shinn, and S. A. Barnett, J. Appl. Phys. **72**, 1805 (1992).

[61] W. Weber, Phys. Rev. B **8**, 5082 (1973).

[62] H. Holleck, J. Vac. Soc. Technol. A **4**, 2661 (1986).

[63] A. Gross, M. Scheffler, M. J. Mehl, and D. A. Papaconstantopoulos, Phys. Rev. Lett. **82**, 1209 (1999).

[64] A. Groß, A. Eichler, J. Hafner, M. J. Mehl, and D. A. Papaconstantopoulos, Surf. Sci. **539**, L542 (2003).

[65] A. C. Luntz, M. D. Williams, and D. S. Bethune, J. Chem. Phys. **89**, 4381 (1988).

[66] P. D. Nolan, B. R. Lutz, P. L. Tanaka, J. E. Davis, and C. B. Mullins, J. Chem. Phys. **111**, 3696 (1999).

[67] D. A. Papaconstantopoulos, M. J. Mehl, S. C. Erwin, and M. R. Pederson, in *Tight-Binding Approach to Computational Materials Science*, edited by P. Turchi, A. Gonis, and L. Colombo (Materials Research Society, Pittsburgh, 1998), Vol. 491, p. 221.

[68] N. Bernstein, M. J. Mehl, D. A. Papaconstantopoulos, N. I. Papanicolaou, M. Z. Bazant, and E. Kaxiras, Phys. Rev. B **62**, 4477 (2000), *erratum* Phys. Rev. B **65**, 249002(E) (2002).

[69] N. Bernstein, H. J. Gotsis, D. A. Papaconstantopoulos, and M. J. Mehl, submitted to *Phys. Rev. B* (unpublished).

[70] D. W. Feldman, J. James H. Parker, W. J. Choyke, and L. Patrick, Phys. Rev. **173**, 787 (1968).

[71] D. A. Papaconstantopoulos and M. J. Mehl, Phys. Rev. B **64**, 172510 (2001).

[72] K.-P. Bohnen, R. Heid, and B. Renker, Phys. Rev. Lett. **86**, 5771 (2001).

[73] I. I. Mazin, D. A. Papaconstantopoulos, and D. J. Singh, Phys. Rev. B **61**, 5223 (2000).

[74] M. D. Johannes, I. I. Mazin, D. J. Singh, and D. A. Papaconstantopoulos, Phys. Rev. Lett. **93**, 101802 (2004).

[75] M. D. Johannes, D. A. Papaconstantopoulos, D. J. Singh, and M. J. Mehl, Europhysics Letters **68**, 433 (2004).

[76] E. Kim, C. Chen, T. Kohler, M. Elstner, and T. Frauenheim, Phys. Rev. Lett. **86**, 652 (2001).

[77] F. Weich, J. Widany, and T. Frauenheim, Phys. Rev. Lett. **78**, 3326 (2001).

[78] P. K. Schelling, N. Yu, and J. W. Halley, Phys. Rev. B **58**, 1279 (1998).

[79] J. W. Halley, Y. Lin, and M. Zhuang, Faraday Discuss. **121**, 85 (2002).

[80] B. C. Pan, Phys. Rev. B **64**, 155408 (2001).